

# Al<sub>2</sub>O<sub>3</sub> and SiO<sub>2</sub> Atomic Layer Deposition Layers on ZnO Photoanodes and Degradation Mechanisms

Qian Cheng,<sup>†</sup> Manpuneet K. Benipal,<sup>†</sup> Qianlang Liu,<sup>†</sup> Xingye Wang,<sup>†</sup> Peter A. Crozier,<sup>†</sup> Candace K. Chan,<sup>\*,†</sup> and Robert J. Nemanich<sup>\*,‡</sup>

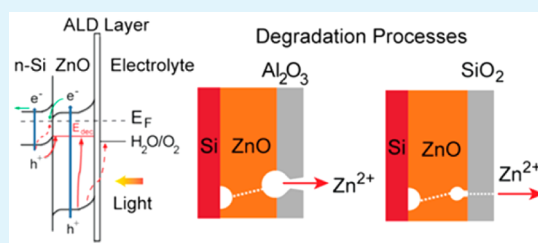
<sup>†</sup>Materials Science and Engineering, School for Engineering of Matter, Transport and Energy, Arizona State University, Tempe, Arizona 85287-6106, United States

<sup>‡</sup>Department of Physics, Arizona State University, Tempe, Arizona 85287-1504, United States

## S Supporting Information

**ABSTRACT:** Strategies for protecting unstable semiconductors include the utilization of surface layers composed of thin films deposited using atomic layer deposition (ALD). The protective layer is expected to (1) be stable against reaction with photogenerated holes, (2) prevent direct contact of the unstable semiconductor with the electrolyte, and (3) prevent the migration of ions through the semiconductor/electrolyte interface, while still allowing photogenerated carriers to transport to the interface and participate in the desired redox reactions. Zinc oxide (ZnO) is an attractive photocatalyst material due to its high absorption coefficient and high carrier mobilities. However, ZnO is chemically unstable and undergoes photocorrosion, which limits its use in applications such as in photoelectrochemical cells for water splitting or photocatalytic water purification. This article describes an investigation of the band alignment, electrochemical properties, and interfacial structure of ZnO coated with Al<sub>2</sub>O<sub>3</sub> and SiO<sub>2</sub> ALD layers. The interface electronic properties were determined using in situ X-ray and UV photoemission spectroscopy, and the photochemical response and stability under voltage bias were determined using linear sweep voltammetry and chronoamperometry. The resulting surface structure and degradation processes were identified using atomic force, scanning electron, and transmission electron microscopy. The suite of characterization tools enable the failure mechanisms to be more clearly discerned. The results show that the rapid photocorrosion of ZnO thin films is only slightly slowed by use of an Al<sub>2</sub>O<sub>3</sub> ALD coating. A 4 nm SiO<sub>2</sub> layer proved to be more effective, but its protection capability could be affected by the diffusion of ions from the electrolyte.

**KEYWORDS:** photoanode, photodegradation, photocorrosion, wide band gap protective layer, interface electronic structure, atomic layer deposition, zinc oxide



## 1. INTRODUCTION

In order to mitigate global warming and control carbon emissions, renewable energy sources have attracted a great deal of attention, with solar water splitting to create hydrogen from water as one promising approach to generate fuels.<sup>1–3</sup> In photoelectrochemical cells, photons incident onto semiconductor photoelectrodes generate electron–hole pairs, which are separated and used in water oxidation and reduction reactions at solid–electrolyte interfaces. Materials used for photoelectrochemical water splitting must have suitable band edges that straddle both H<sup>+</sup>/H<sub>2</sub> and OH<sup>−</sup>/O<sub>2</sub> redox potentials, enable a high reaction rate, and exhibit chemical stability in an aqueous electrolyte.<sup>4</sup>

Thus, far, most of the strategies for protecting unstable semiconductors have utilized protective layers composed of thin films deposited using atomic layer deposition (ALD), as summarized in several recent reviews.<sup>5–9</sup> The protective layer is expected to (1) be stable against reaction with photogenerated holes, (2) prevent direct contact of the unstable semiconductor with the electrolyte, and (3) prevent the migration of ions

through the semiconductor/electrolyte interface, while still allowing photogenerated carriers to transport to the interface and participate in the desired redox reactions. ALD coatings of amorphous TiO<sub>2</sub> have been the most commonly used protective layers. Films as thin as 2 nm were shown to be effective for protecting Si photoanodes, while thicker films (5 nm to >100 nm) have also been used.<sup>10,11</sup> It is believed that the thinner films act as tunneling barriers, whereas defect states or pinholes facilitate charge transfer through the thicker films.

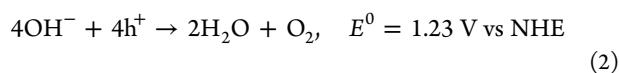
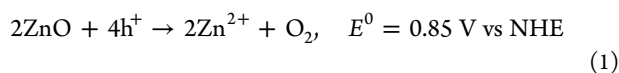
Zinc oxide (ZnO) is an attractive UV-light absorbing photocatalyst material due to its high absorption coefficient and high carrier mobilities, but it suffers from corrosion reactions with photogenerated holes. The energy level for the photocorrosion reaction of ZnO<sup>12</sup> (eq 1) falls in between the conduction and valence band energy levels for ZnO. Hence, it is thermodynamically favorable for photogenerated holes (h<sup>+</sup>)

Received: January 25, 2017

Accepted: April 25, 2017

Published: April 25, 2017

to oxidize ZnO rather than hydroxide ions, which is the desired anodic half-reaction in water splitting (eq 2).



During the photocorrosion process, surface  $\text{O}^{2-}$  react with holes and can become released from the electrode in the form of  $\text{O}_2$ , accompanied by the dissolution of  $\text{Zn}^{2+}$  into the electrolyte (Figure 1A).<sup>13</sup>

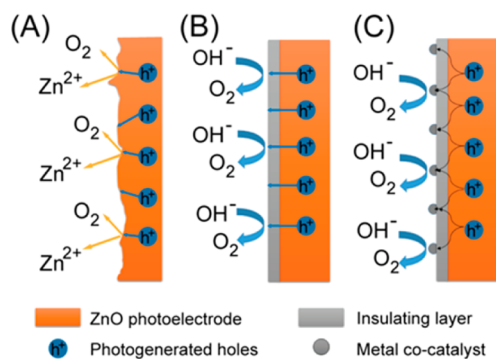


**Figure 1.** Light-induced processes at ZnO/electrolyte interfaces: (A) Bare ZnO surface in which photocorrosion predominates; (B) ZnO coated with an ALD layer, where photogenerated holes can oxidize hydroxide ions to  $\text{O}_2$ ; (C) ZnO coated with metal co-catalyst particles to form a metal-insulator-semiconductor (MIS) structure. In all cases, photogenerated electrons (not shown) are collected at the back contact.

$\text{TiO}_2$  has been investigated as the ALD protective layer for ZnO photoanodes in several studies.<sup>14–16</sup> In the work by Liu et al.,<sup>15</sup> a 1 nm  $\text{TiO}_2$  layer was said to be effective for protecting  $\sim 40$  nm diameter ZnO nanowires from photocorrosion in a 0.1 M KOH electrolyte solution. Furthermore, the  $\text{TiO}_2$  protective layer also passivated the surface states on the ZnO nanowires and removed deep hole traps, leading to an increase in the photocurrent.

However, the use of  $\text{TiO}_2$  as a protective layer for ZnO photoanodes creates potential issues. Due to the lower hole mobility of  $\text{TiO}_2$  compared to ZnO,<sup>17,18</sup> the  $\text{TiO}_2$  layers have to be very thin in order to take advantage of the good hole transport properties of ZnO. Furthermore, the slightly lower valence band maximum (VBM) of  $\text{TiO}_2$  relative to ZnO makes it more favorable for photoexcited holes to migrate toward the ZnO, which could accelerate photocorrosion. Although this effect might be negligible for thin  $\text{TiO}_2$  layers, accelerated photocorrosion was observed in ZnO nanowires coated with 5 nm of conformal  $\text{TiO}_2$  ALD layers that were stored at ambient conditions.<sup>14</sup> In this case, void formation was observed, initiating at the  $\text{TiO}_2/\text{ZnO}$  interface. In contrast,  $\text{Al}_2\text{O}_3$ -coated ZnO nanowires did not show the same kind of instability under ambient storage, presumably because of the absence of photogenerated holes originating from the wide band gap  $\text{Al}_2\text{O}_3$  layer. The deleterious effect of photogenerated holes at the interface between the ZnO and protective layer was illustrated by Li et al.,<sup>19</sup> where ZnO nanowires were protected with a 1.5 nm thick  $\text{Ta}_2\text{O}_5$  ALD layer. Under AM 1.5 irradiation, the insulating  $\text{Ta}_2\text{O}_5$  acted as an effective protective layer for the ZnO, with stability demonstrated for 5 h in a 0.1

M KOH electrolyte. However, when using UV illumination ( $\lambda < 290$  nm) so that the  $\text{Ta}_2\text{O}_5$  ( $E_g = 4.2$  eV) could also absorb light, photocorrosion in the ZnO was observed after 2 h. Similar to  $\text{TiO}_2$ , the valence band of  $\text{Ta}_2\text{O}_5$  is also lower than that for ZnO, which means that photogenerated holes originating from  $\text{Ta}_2\text{O}_5$  could contribute to the photocorrosion of ZnO.

There has also been success in coating ZnO with other light absorbing semiconductors<sup>20</sup> that can protect the ZnO from photocorrosion by preventing direct contact with the electrolyte, while also creating tandem or composite structures with improved charge separation. However, most of these other materials had smaller band gaps than ZnO, which creates an unfavorable light absorption configuration (since the wider band gap semiconductor should usually be on the outermost layer in tandem configurations).

For these reasons, we have chosen to study  $\text{Al}_2\text{O}_3$  and  $\text{SiO}_2$  as insulating protective layers for ZnO photoanodes. Both of these materials are wide band gap insulators with valence band energies much lower than that in ZnO. To our knowledge, there have been limited studies on the use of  $\text{Al}_2\text{O}_3$  and  $\text{SiO}_2$  ALD coatings as protective layers for photoelectrodes.  $\text{Al}_2\text{O}_3$  has been utilized mostly to passivate surface and defect states on high surface area electrodes, such as nanostructured  $\text{Fe}_2\text{O}_3$ ,<sup>21</sup>  $\text{TiO}_2$  nanotubes,<sup>22</sup> and  $\text{WO}_3$  thin films,<sup>23</sup> in order to improve the photoelectrochemical performance. While  $\text{Al}_2\text{O}_3/\text{Fe}_2\text{O}_3$  electrodes were stable in 1 M KOH for  $>30$  min (applied bias of 1.03 V vs RHE under 1 sun illumination)<sup>21</sup> and the  $\text{Al}_2\text{O}_3/\text{TiO}_2$  electrodes were stable for 500 s in 1 M KOH (applied bias of 0.5 V vs Ag/AgCl, 300 W Xe lamp),<sup>22</sup> which was sufficient to demonstrate an enhanced photocurrent. However, the photocorrosion degradation mechanism was not studied in detail. For  $\text{SiO}_2$ , to the best of our knowledge, there have not been detailed studies that have exploited it as a protective layer, and it has not been used in combination with ZnO photoanodes. However, several recent studies have pointed to an important role for  $\text{SiO}_2$  as an “interlayer” between photoanodes and  $\text{TiO}_2$  ALD protective layers in affecting the charge transport to the electrolyte interface.<sup>25–28</sup>

By using  $\text{Al}_2\text{O}_3$  and  $\text{SiO}_2$  as insulating ALD surface layers, charge transfer from the ZnO semiconductor to the electrolyte must occur via uniform charge tunneling across the surface, with hydroxide oxidation occurring near the surface of the ALD layer at the interface with the electrolyte (Figure 1B). This is different from electrodes coated with ALD layers decorated with metal co-catalyst particles, as shown in Figure 1C. In this scenario, the metal-insulator-semiconductor structure (MIS) can enable the photogenerated carriers to tunnel through the dielectric and accumulate at the co-catalyst particles where the electrochemical reaction can take place.<sup>29</sup> For an electrode coated with an ALD layer that is not decorated with co-catalysts, a pinhole or defect in the layer can act as a site for corrosion to initiate; during extended photocatalytic activity, the defect can quickly grow and cause exfoliation of the whole layer. Therefore, it is important to employ various postmeasurement analysis tools to monitor the damage of the ALD layers and elucidate the photocorrosion mechanism.

This article describes an investigation of the interfacial properties and photocorrosion mechanisms of ZnO when coated with amorphous  $\text{Al}_2\text{O}_3$  and  $\text{SiO}_2$  ALD layers. The films were prepared using plasma enhanced atomic layer deposition (PEALD), which is known to deposit films that are more

uniform, dense, conformal, and free from pinholes or impurities compared to layers produced by thermal evaporation or thermal ALD.<sup>30</sup> Model systems consisting of 20 nm ZnO thin films were also deposited using PEALD, which facilitated the investigation of the photocorrosion observations. The electronic properties of the interface between the ZnO electrode and the ALD layers were determined using in situ photoemission spectroscopy in order to understand the band alignment. The photoelectrochemical response and stability were determined using linear sweep voltammetry (LSV) and chronoamperometry (CA), while the degradation processes were identified using atomic force, scanning electron, and transmission electron microscopy.

## 2. EXPERIMENTAL SECTION

More detailed description of the experimental procedures can be found in the [Supporting Information](#). Two different ZnO photoanodes were employed in this research: single crystal ZnO substrates and 20 nm ZnO layers that were deposited using PEALD onto n-type Si (n-Si) or fluorine-doped tin oxide (FTO). The Al<sub>2</sub>O<sub>3</sub> or SiO<sub>2</sub> ALD layers were deposited onto plasma-cleaned ZnO single crystal surfaces or onto the PEALD ZnO surfaces using the same PEALD system.

In situ X-ray photoelectron spectroscopy (XPS) and ultraviolet photoelectron spectroscopy (UPS) were used to characterize the surfaces. The full UPS spectra were recorded to establish the valence band maximum (VBM) and vacuum level position from the low and high binding energy cutoffs, respectively. All measurements were made relative to the system Fermi level. The band alignment of the ALD coating was determined from the core level binding energies and the valence band maximum position using an approach described by Waldrop et al. and Kraut et al.<sup>31,32</sup>

Photoelectrochemical measurements were performed using the ZnO sample as the working electrode, Pt wire as the counter electrode, and a Ag/AgCl reference electrode. The electrolyte solution was 0.1 M K<sub>3</sub>PO<sub>4</sub> with pH adjusted to 7 using H<sub>3</sub>PO<sub>4</sub>. A 450 W Xe solar simulator was used to achieve a light intensity of ~100 mW/cm<sup>2</sup>. Linear sweep voltammetry (LSV) with a 10 mV/s scan rate and chronoamperometry (CA) were used to examine the photocurrent response under chopped light and evaluate the durability of the ZnO electrodes.

To explore the integrity of the SiO<sub>2</sub>, Al<sub>2</sub>O<sub>3</sub>, and ZnO layers after photoelectrochemical measurements, the surface was investigated using atomic force microscopy (AFM) and scanning electron microscopy (SEM). The structure of the interface between the ZnO layer and the ALD layer was examined using cross-sectional transmission electron microscopy (TEM). Precision cross-section samples were prepared with a focused ion beam (FIB) using the lift-out technique.

## 3. RESULTS

**3.1. Al<sub>2</sub>O<sub>3</sub>/ZnO and SiO<sub>2</sub>/ZnO Band Alignment.** To understand the band alignment at the interface between the ALD coatings and ZnO, XPS and UPS measurements were performed on the ALD coated, O-terminated, ZnO single crystal substrates. The relevant scans are shown in [Figures 2A](#) and [3](#). The as-received O-face of ZnO has adsorbed hydrocarbon species and a bonded hydroxyl layer.<sup>33</sup> Thus, surface cleaning is crucial prior to the deposition of the dielectric thin films. On the basis of a series of experiments, we found that annealing at 310 °C in a He:O<sub>2</sub> mixed plasma reduced the amount of surface hydroxyl groups and adsorbed carbon.<sup>33</sup> Specifically, following the plasma clean, the O 1s ([Figure S1](#)) and Zn 2p<sub>3/2</sub> peaks ([Figure 3A](#)) increased in intensity. The high energy shoulder of the O 1s peak was also substantially reduced ([Figure S1B](#)), and the C 1s peak disappeared ([Figure 2B](#)). These results are consistent with

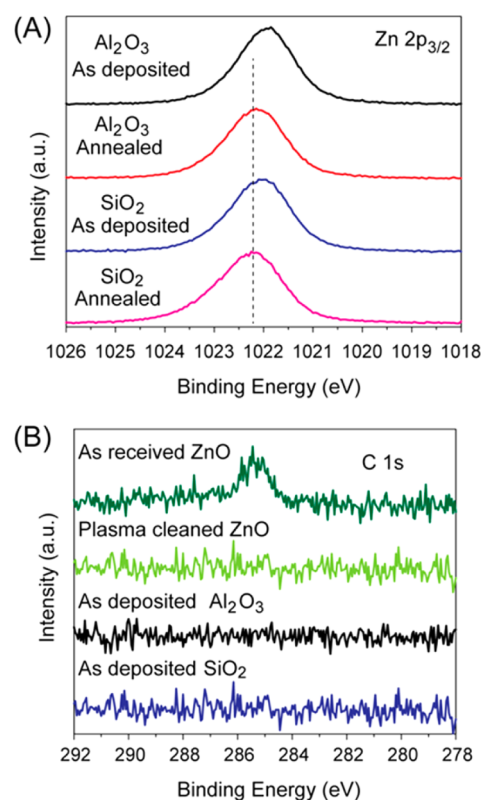


**Figure 2.** XPS spectra of ZnO single crystals (A) showing the Zn 2p<sub>3/2</sub> core level after Al<sub>2</sub>O<sub>3</sub> and SiO<sub>2</sub> deposition and annealing and (B) the C 1s core level after plasma cleaning and Al<sub>2</sub>O<sub>3</sub> and SiO<sub>2</sub> deposition.

removal of the carbon species and a reduction of the hydroxide layer. In addition, after plasma cleaning, the Zn 2p<sub>3/2</sub> core level and ZnO VBM shifted 0.2 eV to lower binding energy ([Figure 3A](#)), which indicated a reduction of the initial downward band bending to essentially flat band conditions.

The band bending is attributed to a space charge layer due to charges at or near the surface or interface. For the initial ZnO substrate surface, the surface-adsorbed hydroxyl groups are believed to act as donors and make the surface positively charged, therefore causing the accumulation of free electrons and downward band bending, as shown in [Figure 4A](#). The small change in work function from 4.3 to 4.5 eV after surface cleaning may also be attributed to removal of the hydroxyl groups.

The XPS and UPS data can be combined and used to draw the band alignment for the heterostructures. The data from the XPS core level (Zn 2p<sub>3/2</sub>, Al 2p, and Si 2p) peak positions and UPS spectra (valence band maximum (VBM) and work function) for ZnO, Al<sub>2</sub>O<sub>3</sub>, and SiO<sub>2</sub> following each clean, deposition, and annealing step are shown in [Figure 3](#) and are included in [Table S1](#). The deduction of the band alignments is outlined in the [Supporting Information](#). The change of band bending during deposition is obtained from shifts of the Al and Si core levels and VBM. After deposition of ~2.0 nm Al<sub>2</sub>O<sub>3</sub> or SiO<sub>2</sub>, upward band bending was indicated in the ZnO, which suggests the presence of negative charge in the PEALD films. Presumably, the negative charge is due to the presence of interstitial oxygen.<sup>34</sup> Postdeposition annealing at 400 °C in research grade N<sub>2</sub> gas apparently removes the oxygen from the thin layers and thus reduces the upward band bending in the ZnO. The band bending is also shown in [Figure 4](#).

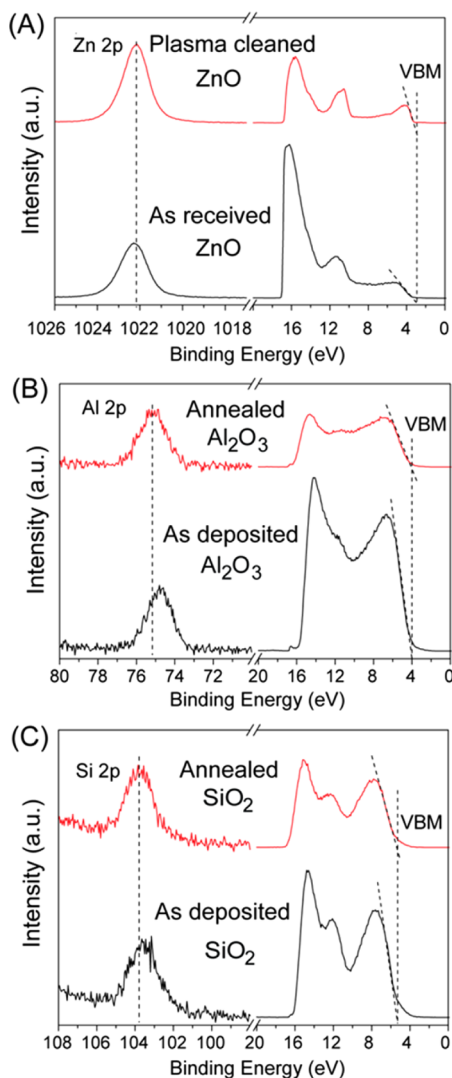


**Figure 3.** XPS Zn 2p<sub>3/2</sub>, Al 2p, or Si 2p core level and UPS spectra (A) of as-received O-face of single crystal ZnO; (B) of as-deposited and annealed Al<sub>2</sub>O<sub>3</sub> PEALD layer on ZnO; (C) of as-deposited and annealed SiO<sub>2</sub> PEALD layer on ZnO.

The band gap of amorphous PEALD Al<sub>2</sub>O<sub>3</sub> was determined to be 6.7 eV from energy loss peaks near the XPS core level,<sup>35</sup> and the reported band gap of amorphous SiO<sub>2</sub> is 8.9 eV.<sup>34</sup> The valence band offset of SiO<sub>2</sub>/ZnO was determined from eq 3, where  $E_{VB}$  is the VBM binding energy,  $E_{CL}$  is core level binding energy, and  $\Delta E_{CL}$  is the difference between the core level binding energies of the ALD layer and the ZnO.

$$\Delta E_{VB} = (E_{CL} - E_{VB})_{ZnO} - (E_{CL} - E_{VB})_{dielectric} + \Delta E_{CL} \quad (3)$$

The obtained experimental values of  $(E_{CL} - E_{VB})_{ZnO}$ ,  $(E_{CL} - E_{VB})_{SiO_2}$ , and  $\Delta E_{CL}$  were 1018.9, 98.2, and -920.7 eV, respectively. Similarly, the values of  $(E_{CL} - E_{VB})_{ZnO}$ ,  $(E_{CL} - E_{VB})_{Al_2O_3}$ , and  $\Delta E_{CL}$  for Al<sub>2</sub>O<sub>3</sub>/ZnO were 1018.9, 70.7, and -947.1 eV, respectively. The values of  $(E_{CL} - E_{VB})$  for Al<sub>2</sub>O<sub>3</sub> and SiO<sub>2</sub> obtained here were similar to those reported in a prior study.<sup>35</sup> The valence and conduction band offsets of the Al<sub>2</sub>O<sub>3</sub>/ZnO heterostructure were 1.1 and 2.2 eV, and for SiO<sub>2</sub>/ZnO, they were 2.5 and 3.2 eV, respectively. The band offsets, electron affinity, and work function are shown in Figure 4. The

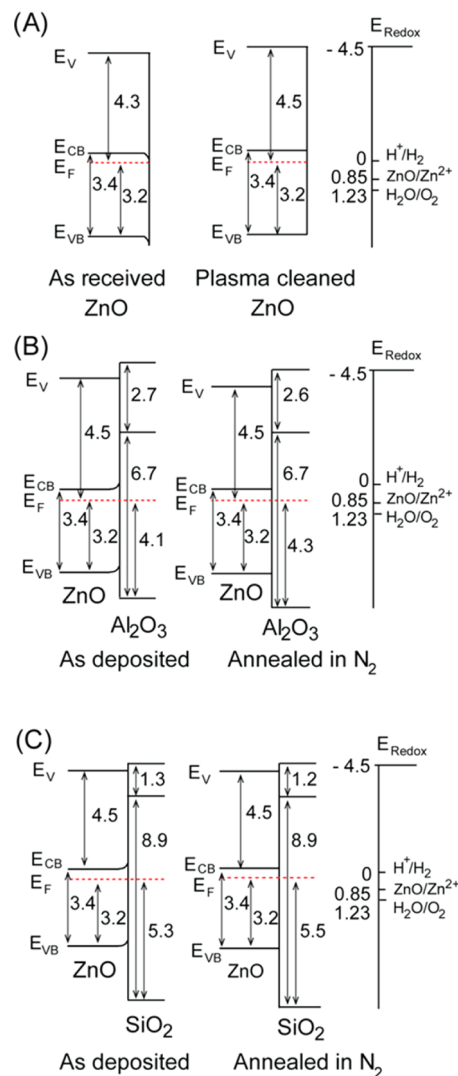


**Figure 4.** Band diagram of (A) O-face of ZnO single crystal: as received and after plasma (He:O<sub>2</sub>) cleaning; (B) PEALD Al<sub>2</sub>O<sub>3</sub>/ZnO: as-deposited and after annealing; (C) PEALD SiO<sub>2</sub>/ZnO: as-deposited and after annealing. All energy values in the band diagrams are in eV. Standard electrode potentials (vs NHE) for H<sup>+</sup>/H<sub>2</sub> (proton reduction), ZnO/Zn<sup>2+</sup> (ZnO corrosion), and H<sub>2</sub>O/O<sub>2</sub> (water oxidation) are shown on the right as reference, with -4.5 eV vs vacuum = 0 V vs NHE.

results show that, for both materials combinations, the band offsets would require tunneling for photoexcited holes originating in ZnO to transit the Al<sub>2</sub>O<sub>3</sub> or SiO<sub>2</sub> layer to the electrolyte.

**3.2. Photoelectrochemical Characterization of Al<sub>2</sub>O<sub>3</sub> and SiO<sub>2</sub> ALD Coatings on PEALD ZnO.** LSV and CA were performed in order to characterize the anodic current resulting from the transport of photogenerated holes from the ZnO to the electrolyte, which could be a result of either a hydroxide oxidation reaction (eq 2) or the undesired ZnO corrosion reaction (eq 1). As shown in Figure 5A, the bare ZnO PEALD thin film showed an anodic photocurrent under LSV scanning. CA was performed at a fixed potential of 0.3 V vs Ag/AgCl to monitor the photocurrent generation over time. The CA test on the bare ZnO film showed an increase in current when the light was turned on, which quickly reached a maximum and then attenuated close to zero within a few minutes (Figure 5B).

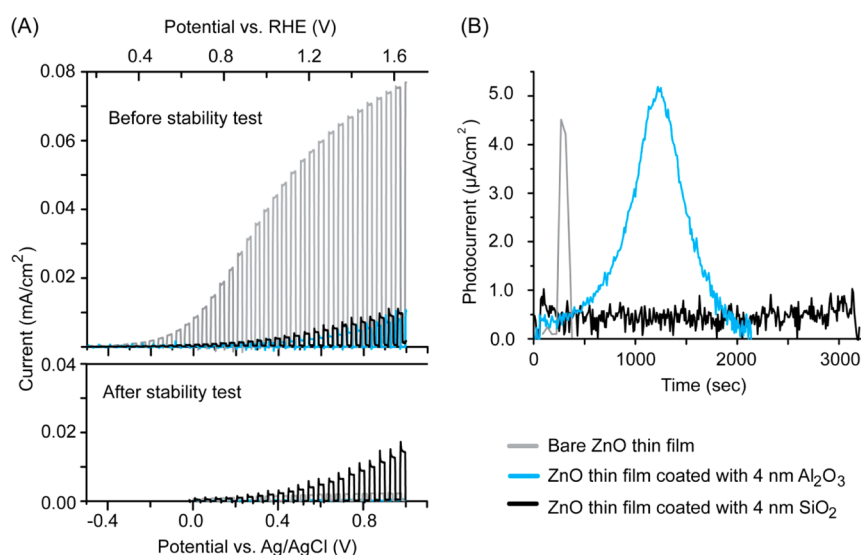


**Figure 5.** Photoelectrochemical measurements of 20 nm ZnO PEALD thin films on FTO substrates as-prepared (bare) and coated with 4 nm  $\text{Al}_2\text{O}_3$  or 4 nm  $\text{SiO}_2$ . (A) LSV under chopped light before and after the CA measurements. (B) Photocurrent from CA stability test with voltage fixed at 0.3 V vs Ag/AgCl.

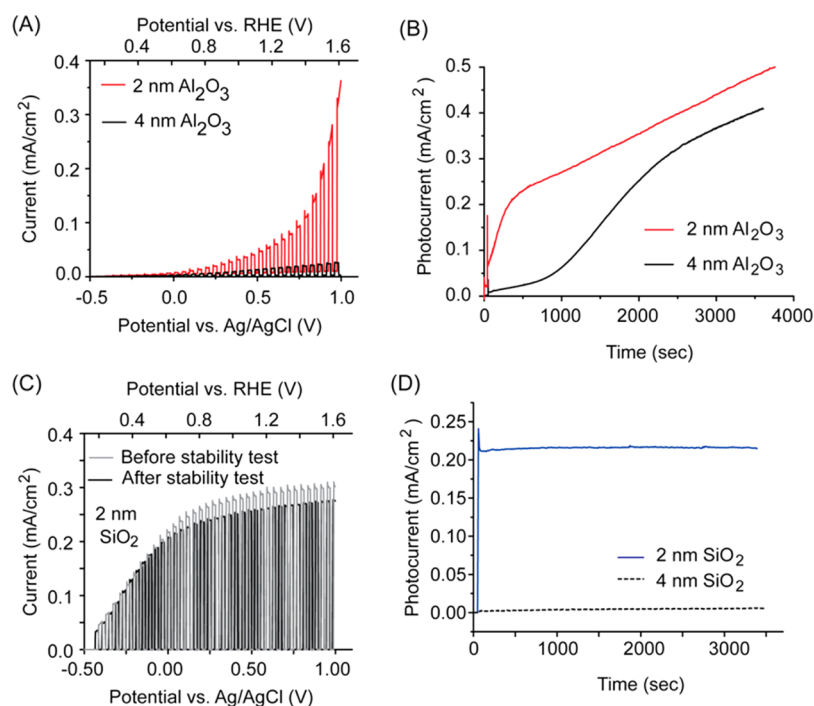


**Figure 6.** Photoelectrochemical measurements of ZnO single crystals coated with (A, B) 2 or 4 nm  $\text{Al}_2\text{O}_3$  and (C, D) 2 or 4 nm  $\text{SiO}_2$ . (A, C) Photocurrent from CA stability test with voltage fixed at 0 V vs Ag/AgCl. (B, D) LSV measurements under chopped light.

The fast rise in photocurrent is attributed to the photocorrosion reactions related to the dissolution of the ZnO, with the decrease in the photocurrent back to zero a result of the removal of ZnO from the FTO substrate. These results indicate that the photocurrent observed in the LSV measurement (Figure 5A) is likely from the photocorrosion of ZnO.

In order to mitigate the photocorrosion reaction, 4 nm layers of either  $\text{Al}_2\text{O}_3$  or  $\text{SiO}_2$  were deposited onto the ZnO. The LSV results showed that the  $\text{SiO}_2$ -coated sample had a slightly higher photocurrent than the  $\text{Al}_2\text{O}_3$ -coated sample, and both of the coated samples had lower photocurrents than the bare ZnO (Figure 5A). Under chopped light illumination, noticeable

transient current spikes followed by decay to a steady state were observed in the LSV plots of the coated ZnO films. Similar “spike and overshoot” transients are commonly observed in photoanodes such as hematite from recombination of carriers at surface states.<sup>36,37</sup> It is not clear if the transient response in our samples arises due to surface recombination (i.e., at the interface between the ALD layer and electrolyte) or due to recombination at the interface between the ALD layer and the ZnO. Regardless, since these transient peaks were less pronounced in the bare ZnO electrodes, we use their appearance as an indication of the presence of the ALD layer on the electrode surface.

When examining the coated ZnO films using the CA stability test, the Al<sub>2</sub>O<sub>3</sub>-coated sample showed only a slight increase in the current once the light was turned on (Figure 5B). However, the photocurrent increased quickly after 300 s and reached a maximum at around 1200 s. As the measurement time increased, the photocurrent started to decrease to zero. After the test, the sample had the same appearance as a bare FTO substrate, indicating that both the ALD layer and the ZnO film had been removed. Hence, the increase and then decrease in photocurrent in the CA results for the Al<sub>2</sub>O<sub>3</sub>-coated sample are also attributed to the photocorrosion and removal of the ZnO, indicating the inability of the Al<sub>2</sub>O<sub>3</sub> layer to sufficiently protect the electrode. On the other hand, the sample coated with SiO<sub>2</sub> maintained a relatively stable photocurrent for the entire duration of the stability test (~1 h), and the color of the substrate surface appeared unchanged after the test.

In order to characterize the electrodes after the CA stability tests, LSV measurements were also performed afterward and compared to the initial LSV curves (Figure 5A). For the bare ZnO and Al<sub>2</sub>O<sub>3</sub>-coated ZnO electrodes, the photocurrent was significantly smaller after the CA test, consistent with the removal of the ZnO layer due to photocorrosion. In contrast, the SiO<sub>2</sub>-coated sample displayed similar photocurrents before and after the CA test and the transient peaks were observed in both curves, suggesting that the SiO<sub>2</sub> layer was intact with the ZnO layer underneath preserved. These results indicate that the photocurrent observed in the LSV and CA curves for the bare and Al<sub>2</sub>O<sub>3</sub>-coated ZnO electrodes were likely originating from the photocorrosion reactions of the ZnO, while the SiO<sub>2</sub> coating was more effective for preventing this process.

The effect of the SiO<sub>2</sub> thickness was also investigated (Figure S3). Decreasing the thickness of the SiO<sub>2</sub> layer resulted in faster photocorrosion. For a ZnO sample coated with 1 nm SiO<sub>2</sub>, a decrease in the photocurrent was observed almost immediately in the CA test (Figure S3A). This suggests that 1 nm of SiO<sub>2</sub> was not sufficient to protect the ZnO surface, thus apparently leading to the exposure of ZnO to the electrolyte and enabling photocorrosion. A ZnO thin film sample coated with 2 nm SiO<sub>2</sub> was stable for ~30 min before the current associated with ZnO photocorrosion started to increase (Figure S3B).

To elucidate the effects of the ALD layers on surfaces with reduced roughness, which could possibly reduce the likelihood of pinhole formation, studies were also performed on ZnO single crystals coated with the Al<sub>2</sub>O<sub>3</sub> and SiO<sub>2</sub> layers. The use of single crystalline substrates could also eliminate the initiation of photocorrosion at grain boundaries. However, due to the increased thickness and light absorbance of the ZnO single crystal, more photogenerated carriers would be produced under light illumination, which could increase the photocorrosion processes. As shown in Figure 6A,C, the LSV measurements on the ZnO single crystals coated with 2 or 4 nm Al<sub>2</sub>O<sub>3</sub> or SiO<sub>2</sub> showed much higher photocurrent compared to the scans for the ZnO PEALD thin films (Figure 5A). The CA stability test was performed on the ZnO single crystal samples with the potential set at 0 V vs Ag/AgCl for 1 h. As shown in Figure 6B, the current continued to increase for both Al<sub>2</sub>O<sub>3</sub> thicknesses and reached values of ~0.5 and ~0.4 mA/cm<sup>2</sup>, respectively, after 1 h. Similar to the electrodes composed of ZnO thin films, this current increase is attributed to the photocorrosion of the ZnO. However, since the ZnO single crystals were much thicker than the ZnO PEALD films, the drop in photocurrent associated with the complete dissolution of ZnO from the electrode was not observed, since the CA testing time was not

long enough for full dissolution of the sample. In contrast to the Al<sub>2</sub>O<sub>3</sub>-coated single crystal, the single crystal with 4 nm SiO<sub>2</sub> coating exhibited very low charge transfer to the electrolyte interface, resulting in very little current (Figure 6D). The sample coated with 2 nm SiO<sub>2</sub> exhibited a slightly lower photocurrent in the LSV measurement after the CA stability test (Figure 6C), but the stable photocurrent of ~0.215 mA/cm<sup>2</sup> in the CA measurement (Figure 6D) suggests that the SiO<sub>2</sub> layer is still essentially intact. These results show that the SiO<sub>2</sub> layer was effective as a protecting layer for ZnO for a range of photocurrent densities.

**3.3. AFM and SEM Characterization.** In order to examine the corrosion mechanism, the 20 nm PEALD ZnO thin films deposited onto n-Si substrates were used, since the n-Si wafers provided flat surfaces for AFM and SEM analysis. The AFM data for the Al<sub>2</sub>O<sub>3</sub>-coated film before and after the CA stability test are shown in Figure 7. The as-prepared Al<sub>2</sub>O<sub>3</sub>-coated sample surface was flat, with roughness (~0.7 nm) similar to the bare ZnO film (Figure 7A).

After CA testing, particles were observed on the electrode surface in both AFM and SEM images, which were attributed to the adhesion of potassium phosphate salts from the electrolyte. Furthermore, pits of different sizes were observed on the surface of the samples after CA measurements of different

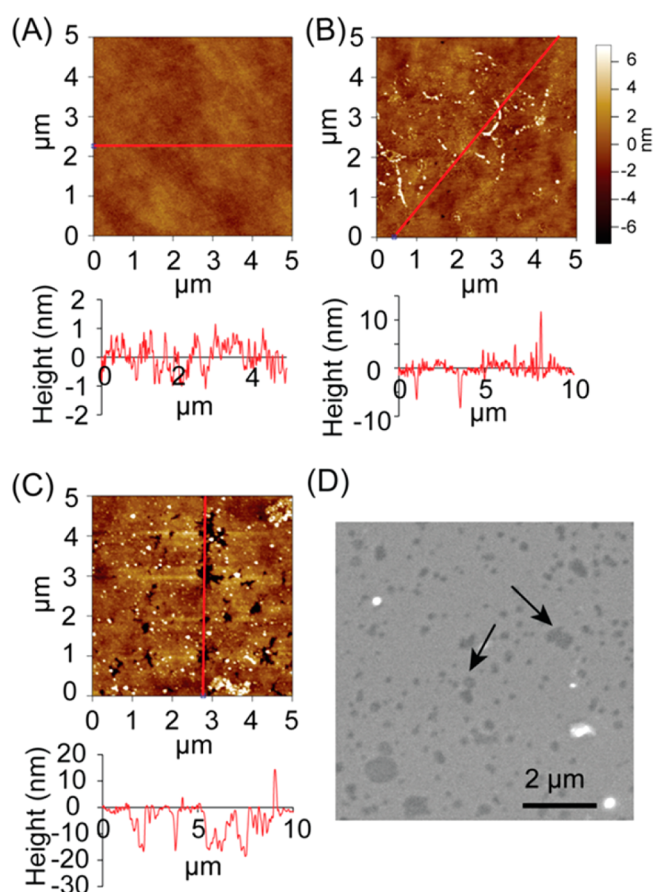


**Figure 7.** AFM and SEM characterization of 20 nm ZnO films deposited onto n-Si and then coated with 4 nm Al<sub>2</sub>O<sub>3</sub>. AFM images (A) before and (B) after the 7 min CA test and (C) after the 15 min CA test. The height profile for each topography image is shown below. (D) SEM image showing the surface morphology of the same sample in (B) after the 7 min CA test. Black arrows indicate the degradation pits.

durations. The AFM scan showed tiny pits  $\sim 6$  nm deep on the surface after performing CA for 7 min, as shown in Figure 7B. AFM imaging of the surface after the 15 min CA test showed an increase in the width and depth of pits (Figure 7C). It is evident from the SEM image (Figure 7D) that the  $\text{Al}_2\text{O}_3$  surface after the 7 min stability test experienced severe damage, with many darker contrast areas present which corresponded to the pits identified in the AFM scans. These results suggest that the degradation of the  $\text{Al}_2\text{O}_3$  layer initiates from pinholes on the surface that expanded into larger sized pits.

On the other hand, AFM observation of the ZnO thin films coated with 4 nm  $\text{SiO}_2$  did not show obvious signs of pitting in the AFM scans, with the surface appearing smooth even after a 1 h CA measurement (Figure 8A,B). The SEM image of the

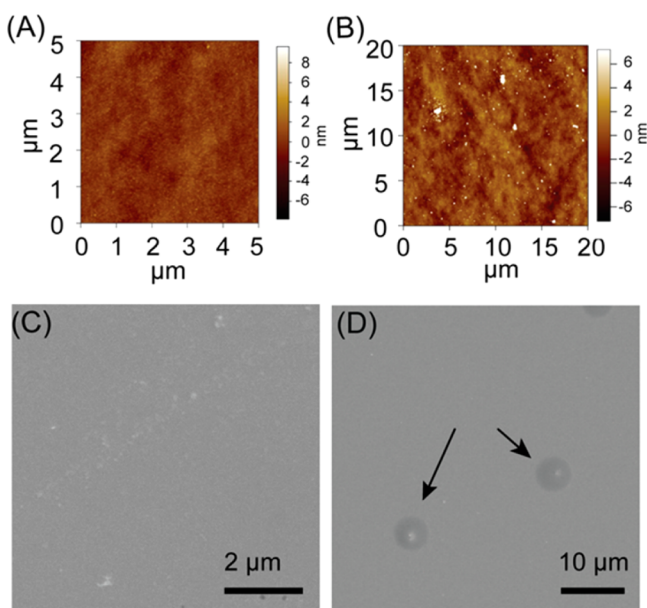


**Figure 8.** AFM and SEM characterization of 20 nm ZnO PEALD films deposited onto n-Si and then coated with 4 nm  $\text{SiO}_2$ . AFM data for the sample (A) as-prepared, and (B) after 1 h durability test. SEM image after CA for (C) 7 min, and (D) 1 h stability test.

$\text{SiO}_2$ -coated sample after 7 min of CA testing (Figure 8C) is notably different from the  $\text{Al}_2\text{O}_3$ -coated sample tested for the same duration (Figure 7D), lacking the dark contrast features associated with the pits. However, in the  $\text{SiO}_2$ -coated sample that underwent the CA test for 1 h, the SEM image revealed a low density of dark circular patches up to  $4 \mu\text{m}$  in diameter with bright centers, as indicated by the black arrows in Figure 8D, which was further investigated using TEM.

**3.4. TEM Characterization.** In order to understand the origin of the features observed in the AFM and SEM images, TEM characterization was performed on cross-sectioned samples to further investigate the failure mechanisms in the  $\text{Al}_2\text{O}_3$  and  $\text{SiO}_2$  films. For the  $\text{Al}_2\text{O}_3$ -coated sample, a section was obtained across a few pits so that the undamaged (Figure 9A) and degraded (Figure 9B) areas could be compared. The  $\sim 21$  nm thick ZnO layer and  $\sim 3$  nm  $\text{Al}_2\text{O}_3$  layer were observed in the undamaged area and confirmed by energy-dispersive X-ray spectroscopy (EDX). The ZnO layer was polycrystalline, while the  $\text{Al}_2\text{O}_3$  layer was amorphous. A thin amorphous layer was observed in between the Si substrate and ZnO thin film and was attributed to the native silicon oxide. Figure 9B is an example of a damaged area where the ZnO layer shows less

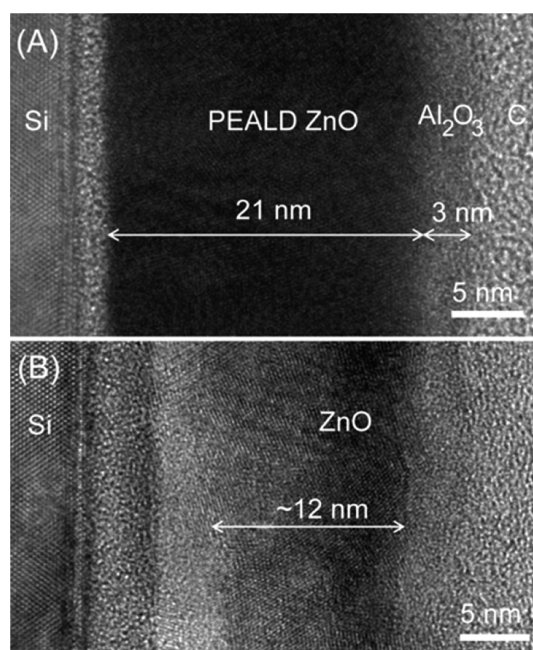


**Figure 9.** TEM cross-sectional image, from the (A) undamaged and (B) damaged areas, showing the microstructure of samples comprising 20 nm ZnO thin films deposited onto n-Si and then coated with 4 nm  $\text{Al}_2\text{O}_3$  (after the 7 min CA stability test).

contrast and a reduced thickness. A contrast gradient was also observed in the ZnO layer here, showing major ZnO loss near the surface of the Si substrate.

Similar analyses were conducted on the sample coated with 4 nm  $\text{SiO}_2$ . From the CA, AFM, and SEM results, this sample displayed slower degradation and fewer dark contrast regions compared to the  $\text{Al}_2\text{O}_3$ -coated sample. A TEM specimen was prepared that included a damaged region from the sample that had undergone CA testing for 1 h. Figure 10A shows an intact area found where a 20 nm uniform layer of polycrystalline ZnO was observed. The 4 nm  $\text{SiO}_2$  layer could not be distinguished from the amorphous carbon (deposited during TEM sample preparation), and EDX was used to confirm the presence of the  $\text{SiO}_2$  layer. An EDX spectrum acquired from the ZnO layer of the intact area showed a predominant Zn L peak and a relatively smaller Si peak, while the spectrum acquired from about 2 nm above the ZnO layer shows a much larger Si peak from the ALD  $\text{SiO}_2$ . The damaged area is also shown in Figure 10B and exhibited a much lighter contrast in the ZnO layer, indicating a smaller thickness in the electron beam direction. Different from the  $\text{Al}_2\text{O}_3$ -coated sample, a relatively uniform contrast in the ZnO was observed in this sample, suggesting a different degradation mechanism which will be discussed in the following section.

## 4. DISCUSSION

The failure mechanism of wide band gap protection layers is attributed to three factors: (1) the deposition of a non-continuous film on the unstable semiconductor, (2) the presence of pinholes in the ALD layer, or (3) diffusion of electrolyte species through the ALD layer to the interface. From the aforementioned described photoelectrochemical results and microscopic observations, it is evident that the  $\text{Al}_2\text{O}_3$  and  $\text{SiO}_2$  ALD films display different properties as surface layers on ZnO photoanodes.

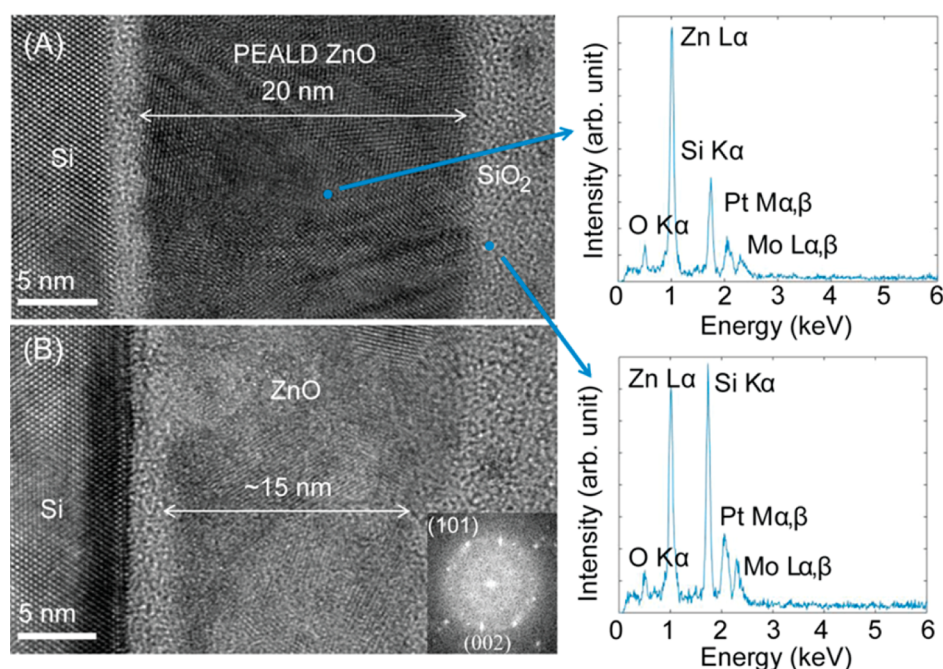


**Figure 10.** TEM cross-sectional image, from the (A) undamaged and (B) damaged areas, showing the microstructure of samples comprising 20 nm ZnO thin films deposited onto n-Si and then coated with 4 nm SiO<sub>2</sub> (after the 1 h CA stability test). The inset in (B) shows the fast Fourier transform (FFT) from the corroded ZnO layer. EDX results from the ZnO layer and the top surface of the undamaged area are also shown. The Pt and Mo peaks in the EDX spectrum come from the process of TEM sample preparation using the FIB technique.

The increase in photocurrent for the Al<sub>2</sub>O<sub>3</sub>-coated ZnO samples (Figures 5B and 6B) during the CA stability tests indicates that degradation still occurs and clearly shows that Al<sub>2</sub>O<sub>3</sub> is not a suitable material to be used as a protective layer for ZnO. The dissolution of Al<sub>2</sub>O<sub>3</sub> ALD layers when immersed in water can cause the thinning of the whole film.<sup>38</sup> The analysis of the AFM and SEM scans shows that the Al<sub>2</sub>O<sub>3</sub>/ZnO surface displays pits after the photoelectrochemical measurements (Figure 7). This implies that pinholes and surface defects in the Al<sub>2</sub>O<sub>3</sub> layer, which may form due to its chemical instability in water, can accelerate the photocorrosion of ZnO at the interface with Al<sub>2</sub>O<sub>3</sub> and cause pitting. These pits can then grow under photoelectrochemical activity and allow the electrolyte ions to contact the ZnO, at which point the photocorrosion reactions can occur (Figure 11A).

In contrast to Al<sub>2</sub>O<sub>3</sub>, SiO<sub>2</sub> showed better stability for the same layer thickness and is more effective for preventing the current increase due to photocorrosion during the CA measurements. If the SiO<sub>2</sub> layer is too thin, then electrolyte diffusion could enable ZnO photocorrosion and removal of the SiO<sub>2</sub> layer. The 4 nm thick SiO<sub>2</sub> layer was more effective for obtaining stable photocurrents in CA measurements, and AFM and SEM characterization after photoelectrochemical tests showed the surface was flat and lacked the same type of pits observed in the Al<sub>2</sub>O<sub>3</sub>-coated samples (Figure 8).

However, the areas of light contrast observed in TEM images (Figure 10B) and a pit-free surface in the AFM image (Figure 8B) implied that degradation of the underlying ZnO was occurring without disturbing the surface of the SiO<sub>2</sub> layer. A similar observation was made in a study by Tomkiewicz et al.,<sup>39</sup> where diffusion of the electrolyte through a 40 nm TiO<sub>2</sub> passivation layer was proposed as the degradation mechanism for the corrosion of the underlying GaAs substrate. In the case of SiO<sub>2</sub>, the diffusion of hydroxide electrolyte species through a SiO<sub>2</sub> layer to the interface with Si was studied with ion diffusion

field effect transistors (ISFETs).<sup>40</sup> Hence, it is feasible for hydroxide ions to diffuse from the electrolyte to the ZnO/SiO<sub>2</sub> interface, which would facilitate the corrosion of ZnO. The Zn<sup>2+</sup> and O<sub>2</sub> could also be released to the electrolyte through this same diffusion process. Therefore, the degradation mechanism of ZnO when covered with SiO<sub>2</sub> is different than that when it is covered with Al<sub>2</sub>O<sub>3</sub>, as shown in Figure 11A,B. The rate of ZnO corrosion when using SiO<sub>2</sub> ALD layers is slowed due to the inhibition of the direct contact between the ZnO and electrolyte liquid. Thus, the SiO<sub>2</sub> layer is better for protecting the ZnO compared to Al<sub>2</sub>O<sub>3</sub>, but corrosion due to the diffusion of ions through the SiO<sub>2</sub> is feasible.

In the TEM analysis of both types of samples, we also observed evidence of reaction and delamination behavior at the interface between the ZnO and n-Si substrate, particularly in the areas where the most severe degradation was observed. We suggest that this observation can be explained by the sample geometry. Due to the wide band gaps of ZnO and the ALD layers, high energy photons will be absorbed in the ZnO, while the longer wavelength photons will excite carriers in the n-Si substrate (Figure 11C). In this type of tandem configuration, photogenerated electrons from ZnO could recombine with the photogenerated holes from n-Si. However, it is also feasible for the photogenerated holes from n-Si, in addition to the photogenerated holes from ZnO, to participate in the decomposition of ZnO at energy level E<sub>dec</sub> as indicated by the red solid arrows in Figure 11C. These two corrosion processes, therefore, result in the thinning of the ZnO layer from both sides, as illustrated in Figure 11A,B.

## 5. CONCLUSIONS

In summary, Al<sub>2</sub>O<sub>3</sub> and SiO<sub>2</sub> ALD layers were deposited onto PEALD ZnO thin films and ZnO single crystals. The ZnO samples coated with SiO<sub>2</sub> showed better stability than those coated with Al<sub>2</sub>O<sub>3</sub>. With the aid of detailed electrochemical and

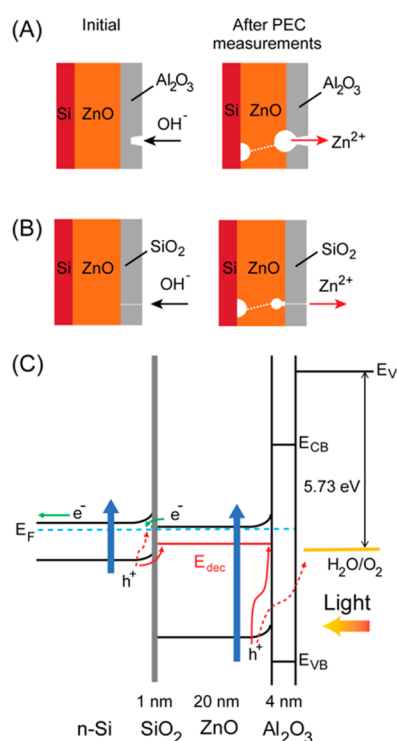


**Figure 11.** Schematic of photodegradation mechanism (A). In  $\text{Al}_2\text{O}_3$ -coated ZnO, the chemical instability of  $\text{Al}_2\text{O}_3$  in water facilitates its dissolution and enables pinholes to grow, allowing direct contact of ZnO with the electrolyte and its photocorrosion.  $\text{Zn}^{2+}$  ions from the corroded ZnO can leave through the pinholes. (B) In  $\text{SiO}_2$ -coated ZnO, electrolyte ions diffuse through the  $\text{SiO}_2$  layer and  $\text{Zn}^{2+}$  can likely diffuse out. In both samples, photogenerated holes in the n-Si substrate can also cause reactions at the n-Si/ZnO interface. (C) Schematic of energy band diagram of the n-Si/ZnO/ $\text{Al}_2\text{O}_3$  sample (see the Supporting Information) and the interface with the electrolyte. Under light irradiation, photoexcited carriers (blue arrows) are generated in both n-Si and ZnO. Green arrows indicate electron drift and trapping and red dashed arrows indicate hole drift and trapping. The red dashed arrow at the surface shows water oxidation (at the standard electrochemical potential), and the red solid arrows show processes that may lead to ZnO degradation and photocorrosion.

microscopic characterization, particularly TEM, the degradation mechanisms were studied. The inability of the  $\text{Al}_2\text{O}_3$  layer to protect ZnO from photocorrosion stems from its chemical instability, which can lead to the formation of pinholes or defects that grow under light irradiation to form corrosion pits in the ZnO. Although the sample coated with 4 nm of  $\text{SiO}_2$  showed better stability, TEM analysis after photoelectrochemical measurements suggested that diffusion of ions from the electrolyte through the  $\text{SiO}_2$  layer may contribute to corrosion of the underlying ZnO layer. The importance of light absorption by other layers in the sample was also discerned, as light absorption by the n-Si substrate led to unintended degradation at the interface with ZnO farthest away from the electrolyte. The results presented here suggest the development of wide band gap protective layers that are both stable in the electrolyte and limit ion diffusion would be advantageous.

## ■ ASSOCIATED CONTENT

### Supporting Information

The Supporting Information is available free of charge on the ACS Publications website at DOI: 10.1021/acsami.7b01274.

Detailed description of sample preparation and characterization. Table with summary of XPS and UPS data. XPS O 1s spectrum of ZnO single crystal as-received and after plasma cleaning. XPS Zn 2p, O 1s, and Al 2p spectra from PEALD ZnO after coating with  $\text{Al}_2\text{O}_3$ . CA measurements of 1 and 2 nm  $\text{SiO}_2$  deposited onto 20 nm ZnO PEALD films on FTO (PDF)

## ■ AUTHOR INFORMATION

### Corresponding Authors

\*E-mail: [candace.chan@asu.edu](mailto:candace.chan@asu.edu) (C.K.C.).

\*E-mail: [robert.nemanich@asu.edu](mailto:robert.nemanich@asu.edu) (R.J.N.).

### ORCID

Peter A. Crozier: 0000-0002-1837-2481

Candace K. Chan: 0000-0003-4329-4865

### Author Contributions

The manuscript was written through contributions of all authors. Q.C. performed the photoelectrochemical measurements; M.K.B. performed the surface cleaning and ALD depositions, AFM scans, and XPS/UPS measurements; Q.L. performed the electron microscopy; and X.W. performed ALD depositions and XPS measurements. All authors have given approval to the final version of the manuscript.

### Notes

The authors declare no competing financial interest.

## ■ ACKNOWLEDGMENTS

This research was supported by the Arizona Board of Regents (ABOR) as part of the Tri-University Advanced Materials Project and Arizona Center of Excellence for Energy Conversion and Storage Technologies (CEECaST). R.J.N., M.K.B., and X.W. acknowledge support from the NSF (DMR 1206935). Q.L. and P.A.C. acknowledge support from the U.S. Department of Energy (DE-SC0004954). The authors would like to thank D. Buttry, X. Peng, and A. Copple for helpful discussions. The authors gratefully acknowledge the use of facilities within the LeRoy Eyring Center for Solid State Science at Arizona State University.

## ■ REFERENCES

- (1) Maeda, K.; Teramura, K.; Lu, D.; Takata, T.; Saito, N.; Inoue, Y.; Domen, K. Photocatalyst Releasing Hydrogen from Water. *Nature* **2006**, *440*, 295–295.
- (2) Grätzel, M. Photoelectrochemical Cells. *Nature* **2001**, *414*, 338–344.
- (3) Sasaki, Y.; Nemoto, H.; Saito, K.; Kudo, A. Solar Water Splitting using Powdered Photocatalysts Driven by Z-schematic Interparticle Electron Transfer without an Electron Mediator. *J. Phys. Chem. C* **2009**, *113*, 17536–17542.
- (4) Walter, M. G.; Warren, E. L.; McKone, J. R.; Boettcher, S. W.; Mi, Q.; Santori, E. A.; Lewis, N. S. Solar Water Splitting Cells. *Chem. Rev.* **2010**, *110*, 6446–6473.
- (5) Singh, T.; Lehnen, T.; Leuning, T.; Mathur, S. Atomic Layer Deposition Grown  $\text{MO}_x$  Thin Films for Solar Water Splitting: Prospects and Challenges. *J. Vac. Sci. Technol., A* **2015**, *33*, 010801.
- (6) Hu, S.; Lewis, N. S.; Ager, J. W.; Yang, J.; McKone, J. R.; Strandwitz, N. C. Thin-Film Materials for the Protection of Semiconducting Photoelectrodes in Solar-Fuel Generators. *J. Phys. Chem. C* **2015**, *119*, 24201–24228.
- (7) Guijarro, N.; Prévot, M. S.; Sivula, K. Surface Modification of Semiconductor Photoelectrodes. *Phys. Chem. Chem. Phys.* **2015**, *17*, 15655–15674.
- (8) Lichterman, M. F.; Sun, K.; Hu, S.; Zhou, X.; McDowell, M. T.; Shaner, M. R.; Richter, M. H.; Crumlin, E. J.; Carim, A. I.; Saadi, F. H.;

Brunschwig, B. S.; Lewis, N. S. Protection of Inorganic Semiconductors for Sustained, Efficient Photoelectrochemical Water Oxidation. *Catal. Today* **2016**, *262*, 11–23.

(9) Scheuermann, A. G.; McIntyre, P. C. Atomic Layer Deposited Corrosion Protection: A Path to Stable and Efficient Photoelectrochemical Cells. *J. Phys. Chem. Lett.* **2016**, *7*, 2867–2878.

(10) Lee, M. H.; Takei, K.; Zhang, J.; Kapadia, R.; Zheng, M.; Chen, Y.; Nah, J.; Matthews, T. S.; Chueh, Y.; Ager, J. W.; Javey, A. p-Type InP Nanopillar Photocathodes for Efficient Solar-Driven Hydrogen Production. *Angew. Chem.* **2012**, *124*, 10918–10922.

(11) Hu, S.; Shaner, M. R.; Beardslee, J. A.; Lichterman, M.; Brunschwig, B. S.; Lewis, N. S. Amorphous TiO<sub>2</sub> Coatings Stabilize Si, GaAs, and GaP Photoanodes for Efficient Water Oxidation. *Science* **2014**, *344*, 1005–1009.

(12) Gerischer, H. On the Stability of Semiconductor Electrodes Against Photodecomposition. *J. Electroanal. Chem. Interfacial Electrochem.* **1977**, *82*, 133–143.

(13) Gerischer, H. Electrochemical Behavior of Semiconductors under Illumination. *J. Electrochem. Soc.* **1966**, *113*, 1174–1182.

(14) Yang, Y.; Kim, D. S.; Qin, Y.; Berger, A.; Scholz, R.; Kim, H.; Knez, M.; Gösele, U. Unexpected Long-Term Instability of ZnO Nanowires “Protected” by a TiO<sub>2</sub> Shell. *J. Am. Chem. Soc.* **2009**, *131*, 13920–13921.

(15) Liu, M.; Nam, C.; Black, C. T.; Kamcev, J.; Zhang, L. Enhancing Water Splitting Activity and Chemical Stability of Zinc Oxide Nanowire Photoanodes with Ultrathin Titania Shells. *J. Phys. Chem. C* **2013**, *117*, 13396–13402.

(16) Kayaci, F.; Vempati, S.; Ozgit-Akgun, C.; Donmez, I.; Biyikli, N.; Uyar, T. Selective Isolation of the Electron or Hole in Photocatalysis: ZnO–TiO<sub>2</sub> and TiO<sub>2</sub>–ZnO Core–Shell Structured Heterojunction Nanofibers via Electrospinning and Atomic Layer Deposition. *Nanoscale* **2014**, *6*, 5735–5745.

(17) Look, D. C.; Reynolds, D. C.; Sizelove, J.; Jones, R.; Litton, C. W.; Cantwell, G.; Harsch, W. Electrical Properties of Bulk ZnO. *Solid State Commun.* **1998**, *105*, 399–401.

(18) Liu, M.; Nam, C.; Black, C. T.; Kamcev, J.; Zhang, L. Enhancing Water Splitting Activity and Chemical Stability of Zinc Oxide Nanowire Photoanodes with Ultrathin Titania Shells. *J. Phys. Chem. C* **2013**, *117*, 13396–13402.

(19) Li, C.; Wang, T.; Luo, Z.; Zhang, D.; Gong, J. Transparent ALD-grown Ta<sub>2</sub>O<sub>5</sub> Protective Layer for Highly Stable ZnO Photoelectrode in Solar Water Splitting. *Chem. Commun.* **2015**, *51*, 7290–7293.

(20) Li, Y.; Zhang, X.; Jiang, S.; Dai, H.; Sun, X.; Li, Y. Improved Photoelectrochemical Property of a Nanocomposite NiO/CdS@ ZnO Photoanode for Water Splitting. *Sol. Energy Mater. Sol. Cells* **2015**, *132*, 40–46.

(21) Le Formal, F.; Tétreault, N.; Cornuz, M.; Moehl, T.; Grätzel, M.; Sivula, K. Passivating Surface States on Water Splitting Hematite Photoanodes with Alumina Overlayers. *Chem. Sci.* **2011**, *2*, 737–743.

(22) Gui, Q.; Xu, Z.; Zhang, H.; Cheng, C.; Zhu, X.; Yin, M.; Song, Y.; Lu, L.; Chen, X.; Li, D. Enhanced Photoelectrochemical Water Splitting Performance of Anodic TiO<sub>2</sub> Nanotube Arrays by Surface Passivation. *ACS Appl. Mater. Interfaces* **2014**, *6*, 17053–17058.

(23) Kim, W.; Tachikawa, T.; Monllor-Satoca, D.; Kim, H.; Majima, T.; Choi, W. Promoting Water Photooxidation on Transparent WO<sub>3</sub> Thin Films using an Alumina Overlayer. *Energy Environ. Sci.* **2013**, *6*, 3732–3739.

(24) Barpuzary, D.; Khan, Z.; Vinothkumar, N.; De, M.; Qureshi, M. Hierarchically Grown Urchinlike CdS@ ZnO and CdS@ Al<sub>2</sub>O<sub>3</sub> Heteroarrays for Efficient Visible-Light-Driven Photocatalytic Hydrogen Generation. *J. Phys. Chem. C* **2012**, *116*, 150–156.

(25) Kenney, M. J.; Gong, M.; Li, Y.; Wu, J. Z.; Feng, J.; Lanza, M.; Dai, H. High-Performance Silicon Photoanodes Passivated with Ultrathin Nickel Films for Water Oxidation. *Science* **2013**, *342*, 836–840.

(26) Scheuermann, A. G.; Lawrence, J. P.; Kemp, K. W.; Ito, T.; Walsh, A.; Chidsey, C. E. D.; Hurley, P. K.; McIntyre, P. C. Design

Principles for Maximizing Photovoltage in Metal-Oxide-Protected Water-Splitting Photoanodes. *Nat. Mater.* **2016**, *15*, 99–105.

(27) Scheuermann, A. G.; Kemp, K. W.; Tang, K.; Lu, D. Q.; Satterthwaite, P. F.; Ito, T.; Chidsey, C. E. D.; McIntyre, P. C. Conductance and Capacitance of Bilayer Protective Oxides for Silicon Water Splitting Anodes. *Energy Environ. Sci.* **2016**, *9*, 504–516.

(28) Satterthwaite, P. F.; Scheuermann, A. G.; Hurley, P. K.; Chidsey, C. E. D.; McIntyre, P. C. Engineering Interfacial Silicon Dioxide for Improved Metal-Insulator-Semiconductor Silicon Photoanode Water Splitting Performance. *ACS Appl. Mater. Interfaces* **2016**, *8*, 13140–13149.

(29) Esposito, D. V.; Levin, I.; Moffat, T. P.; Talin, A. A. H<sub>2</sub> evolution at Si-based Metal–Insulator–Semiconductor Photoelectrodes Enhanced by Inversion Channel Charge Collection and H Spillover. *Nat. Mater.* **2013**, *12*, 562–568.

(30) George, S. M. Atomic Layer Deposition: An Overview. *Chem. Rev.* **2010**, *110*, 111–131.

(31) Waldrop, J.; Grant, R. Measurement of AlN/GaN (0001) Heterojunction Band Offsets by X-Ray Photoemission Spectroscopy. *Appl. Phys. Lett.* **1996**, *68*, 2879–2881.

(32) Kraut, A.; Grant, R. W.; Waldrop, J. R.; Kowalczyk, S. P. In *Heterojunction Band Discontinuities: Physics and Device Applications*; Capasso, F., Margaritondo, G., Eds.; Elsevier: New York, 1987.

(33) Coppa, B. J.; Fulton, C. C.; Hartlieb, P. J.; Davis, R. F.; Rodriguez, B. J.; Shields, B. J.; Nemanich, R. J. In Situ Cleaning and Characterization of Oxygen- and Zinc-Terminated, n-Type, ZnO (0001) Surfaces. *J. Appl. Phys.* **2004**, *95*, 5856.

(34) Yang, J.; Eller, B. S.; Nemanich, R. J. Surface Band Bending and Band Alignment of Plasma Enhanced Atomic Layer Deposited Dielectrics on Ga- and N-Face Gallium Nitride. *J. Appl. Phys.* **2014**, *116*, 123702.

(35) Yang, J.; Eller, B. S.; Kaur, M.; Nemanich, R. J. Characterization of Plasma-Enhanced Atomic Layer Deposition of Al<sub>2</sub>O<sub>3</sub> using Dimethylaluminum Isopropoxide. *J. Vac. Sci. Technol., A* **2014**, *32*, 021514.

(36) Peter, L. M.; Upul Wijayantha, K. G.; Tahir, A. A. Kinetics of Light-Driven Oxygen Evolution at  $\alpha$ -Fe<sub>2</sub>O<sub>3</sub> Electrodes. *Faraday Discuss.* **2012**, *155*, 309–322.

(37) Peter, L. M. Energetics and Kinetics of Light-Driven Oxygen Evolution at Semiconductor Electrodes: The Example of Hematite. *J. Solid State Electrochem.* **2013**, *17*, 315–326.

(38) Abdulagatov, A.; Yan, Y.; Cooper, J.; Zhang, Y.; Gibbs, Z.; Cavanagh, A.; Yang, R.; Lee, Y.; George, S. Al<sub>2</sub>O<sub>3</sub> and TiO<sub>2</sub> Atomic Layer Deposition on Copper for Water Corrosion Resistance. *ACS Appl. Mater. Interfaces* **2011**, *3*, 4593–4601.

(39) Tomkiewicz, M.; Woodall, J. M. Photoelectrolysis of Water with Semiconductor Materials. *J. Electrochem. Soc.* **1977**, *124*, 1436–1440.

(40) Topkar, A.; Lal, R. Effect of Electrolyte Exposure on Silicon Dioxide in Electrolyte-Oxide-Semiconductor Structures. *Thin Solid Films* **1993**, *232*, 265–270.